Journal of Thermal Analysis and Calorimetry (2022) 147:9793–9809
https://doi.org/10.1007/s10973-022-11208-8

Prediction of combustion reactivity for lignocellulosic fuels by means of machine learning

Senem Sezer[1] · Furkan Kartal[1] · Uğur Özveren[1]

Received: 7 May 2021 / Accepted: 4 January 2022 / Published online: 7 February 2022

Abstract
Energy demand and environmental concerns made biomass a sustainable energy source that can be used as a substitute for coal in many applications. Therefore, the combustion efficiency of biomass is a major concern for policy makers and engineers. Thermogravimetric analysis (TGA) is a robust method for determining the combustion characteristics of biomass using combustion index. TGA instruments, on the other hand, are quite expensive, and performing the experiments themselves requires a lot of time and a trained operator. Developing a method that is both faster and more reliable to obtain combustion characteristics without the use of TGA is therefore very important. In this study, a machine learning approach based on artificial neural network (ANN) was developed to predict the instantaneous combustion index defined for biomass combustion process with the help of biomass properties and combustion conditions, without using instruments and complex equations. Thus, a total of 6721 data sets were generated by using the 24 thermogravimetric experiments which conducted in this work. The Bayesian regularization optimization algorithm was used to train the developed ANN model, which is based on a multilayer perceptron architecture. The results showed that there was good agreement between the predicted and measured values of the combustion index for the training, testing, and external validation data sets. The mean absolute percentage error (MAPE), regression coefficient (R^2), root-mean-square error (RMSE) for each biomass sample under the different experimental conditions were investigated, and the results were found to be satisfactory with $R^2 > 0.99$.

Keywords Artificial neural network · Combustion · Biomass · Instantaneous combustion index · Thermogravimetric analysis

Introduction

The energy demand of modern society is continuously increasing in parallel with industrial development and population growth [1]. About 80 percent of this immense demand is met by fossil fuels [2]. Although direct combustion of coal, one of the most widely used fossil fuels, is often preferred for power generation, coal has several negative environmental impacts associated with mining, processing, transportation, and combustion. Moreover, the increase in CO_2 concentration in the atmosphere as a result of fossil fuel combustion is considered to be the main cause of climate change [3]. Biomass, on the other hand, is the only renewable energy source that has the potential to be employed as a replacement for coal in a wide range of applications. In addition, biomass is an attractive renewable energy source because it is abundant, cheap and a sustainable fuel [4].

During biomass combustion processes, the production of ash is less; further, lower quantities of NO_x and SO_x are emitted compared to coal burning. Additionally, biomass consumes CO_2 during their own growth stages, and they do not increase CO_2 in the atmosphere when combusted [5]. Also, the three major biocomponents (cellulose, hemicellulose, and lignin) representing the organic structure of biomass are easy to decompose by applying heat treatment [6, 7]. Coal, on the other hand, is difficult to deal with in monocombustion processes due to its high ignition temperature and low volatile content. Consequently, biomass combustion is a remarkably efficient and effective technique in terms of getting rid of biomass waste, providing energy recovery, and destruction of toxic organic compounds [8].

Because of all these properties stated above, biomass is a unique renewable fuel whose burning characteristic is

✉ Uğur Özveren
ugur.ozveren@marmara.edu.tr

[1] Department of Chemical Engineering, Marmara University, Goztepe Campus, 34722 Kadikoy, Turkey

significant to examine. Thermogravimetric analysis (TGA) has been frequently used to acquire combustion characteristic data for solid fuels [9–11]. Numerous properties of the combustion behavior of lignocellulosic fuels have been analyzed using this technique because it offers a relatively small-scale, simple, cheaper, fast, and reliable way to obtain the ignition profiles of solid fuels [12]. Moreover, with the TGA method, not only combustion but many thermolysis processes can be investigated under various conditions (e.g., atmosphere, heating rate, and temperature). In non-isothermal TGA, feedstock samples are generally heated to around 800–1000°C at various heating rates [13]. The measured decrease in mass due to thermal decomposition is continuously recorded. As a result of the analysis, many parameters regarding the thermolysis procedure of the fuel sample can be evaluated such as ignition/burnout temperatures, decomposition rate, comprehensive combustion index, peak temperatures, and residual mass [14]. Moreover, kinetic parameters (reaction order, pre-exponential factor, and activation energy) are derived by applying quantitative methods to TG curves [15]. This information is of great importance in terms of increasing the knowledge about a system or power plant, enhancing efficiency, accurate design of equipment, and determining optimum process conditions. Recently, numerous researchers are developing computerized approaches to reduce the number of experiments performed in the laboratory. Researchers have been worked on many correlations and other computational techniques for energy systems to save time and cost. Artificial neural networks as a machine learning techniques have been substantially accepted to overcome complicated problems due to their influence on mapping nonlinear patterns. Xie et al. [16] characterized the co-combustion of pomelo peel and textile dyeing sludge blend using TGA under the six different atmospheres. Researchers predicted TGA data under the different O_2/CO_2 atmospheres by applying radial basis and Bayesian regularized artificial neural network. Similarly, Chen et al. [17] predicted TG curves for co-combustion of coffee grounds and sewage-sludge blends using ANN. Furthermore, Díaz-Faes et al. [18] developed a model to predict the coke strength after reaction using TGA parameters. The authors stated that the developed model which is derived from the thermogravimetric analysis of coals can be used in coke quality estimation. In another work, Çepelioğullar et al. [19] established different ANNs that predict the activation energy for TGA applications. In neural networks estimating the activation energy based on different kinetic models, the temperature and heating rate were chosen in the input layer, and olive oil residues and lignocellulosic forest residues were used as fuel. However, the ANN models developed in these studies are specific to one or two particular types of biomass and are not universal.

Although many parameters of TGA have been estimated by various researchers, to the best of our knowledge, no study has been conducted to estimate the instantaneous combustion index using a machine learning approach. The objective of this study is to develop an ANN model as a machine learning approach that estimates the instantaneous combustion index of biomass combustion process based on fuel properties and operating conditions without using an instrument and complex equations. In previous studies, a single combustion index was estimated for a specific combustion zone, whereas in this study, the combustion index at each individual temperature was calculated for the entire combustion zone. The experimental and modeling procedures adopted for this work can be summarized as follows: (i) characterization of fuels (proximate and elemental analyses), (ii) preparation of biomass samples (drying, grinding, and screening), (iii) non-isothermal combustion experiments using TGA (ignition/combustion profiles and peak temperature), (iv) determination of input parameters for the ANN model (heating rate, temperature, carbon, hydrogen, and oxygen content (mass%, on dry basis)), (v) training of the ANN model, (vi) evaluation of the performance of the ANN model for test and external experimental validation data sets.

Materials and methods

Sample

The feedstock materials used in this study, which are hazelnut shell, hazelnut husk, almond shell, barley straw, wheat straw, olive pomace, rice husk, and rice straw, were supplied from local farmers in Turkey. The proximate and elemental analyses of biomass materials were executed according to American Society for Testing and Materials (ASTM) standards. The thermogravimetric analyzer NETZSCH 409 PC Luxx from NETZSCH-Feinmahltechnik GmbH was used to perform the proximate analysis. Furthermore, LECO Truspec brand microelemental analyzer was used to obtain elemental analysis results (C, H, N, and S) from Hacettepe University. However, the oxygen content of biomass is calculated as follows:

$$O(\%) = 100 - (C + H + N + S + ASH) \quad (1)$$

where C, H, N, and S represent mass percentages (mass %, on a dry basis) of carbon, hydrogen, nitrogen, and sulfur, and ASH is ash content (mass %, on a dry basis) of biomass. The results of the proximate and elemental analyses are summarized in Table 1.

Table 1 Proximate analysis and elemental analysis results of the biomass samples

Proximate analysis result	Hazelnut shell	Hazelnut husk	Almond shell	Barley straw	Wheat straw	Olive pomace	Rice husk	Rice straw
Moisture	3.07	3.96	2.27	2.68	2.35	3.08	3.92	2.73
Volatile matter	70.76	64.45	76.51	69.67	67.71	68.60	63.10	68.70
Fixed carbon	25.32	22.89	20.02	14.14	15.52	21.51	13.86	14.77
Ash	0.85	8.70	1.20	13.51	14.42	6.81	19.12	13.80
Elemental analysis result								
C	41.65	41.39	45.16	36.40	36.83	47.40	37.49	39.44
H	5.58	5.27	5.72	5.12	5.12	5.73	5.15	5.27
O	49.05	41.27	44.70	41.03	40.34	36.17	35.03	38.18
N	0.50	0.86	0.15	0.49	0.74	1.54	0.89	0.81
S	2.34	2.15	3.04	3.07	2.19	2.14	1.54	2.11

The quantity of elements gives different characteristics to the solid fuel structure. H, C, and O contents of the solid fuel are the most important parameters for classifying them as biomass, coal, and other types. The plots of O/C versus H/C of the fuel samples using elemental analysis are shown in Fig. 1.

Biomass samples were placed in the biomass circle according to their different O/C and H/C ratios, as shown in Fig. 1. Hazelnut shell (HS) with a higher percentage of O was located on the right side of the biomass circle with a high O/C ratio, while the olive pomace (OP) was placed on the left side of the biomass circle with its high C and relatively low O contents. The combustion characteristics of the biomass samples that are near each other with similar C, H, and O content, such as almond shell (AS), hazelnut husk (HH), and rice shell (RS), are expected to be more similar compared with the others. The biomass samples were clustered into three regions according to their similar O/C and H/C ratios. One of them has only olive pomace (OP), which has the lowest O/C and H/C ratio. The second group has almond shell (AS), hazelnut husk (HH), and rice shell (RS) and rice husk (RH), and the other group consists of wheat straw (WS), barley straw (BS), and hazelnut shell (HS).

Thermogravimetric analysis

Biomass samples were dried at 105°C for 24 h, then ground, and sieved below 250 µm before thermogravimetric analysis (TGA). The "IKA M20 Universal Mill" was used to grind all biomass samples. TGA experiments were conducted in a commercial "Netzsch 409 PC Luxx" apparatus as shown in Fig. 2. An Al_2O_3 crucible containing approximately 10.000 ± 1.000 mg of biomass sample was utilized for each experiment. A flow rate of 45 mL min^{-1} of argon (79%) and oxygen (21%) was used in all combustion experiments.

Non-isothermal combustion experiments were also carried out at heating rates of 10°C min^{-1}, 20°C min^{-1}, and 40°C min^{-1} between 200 and 800°C. Differential thermal

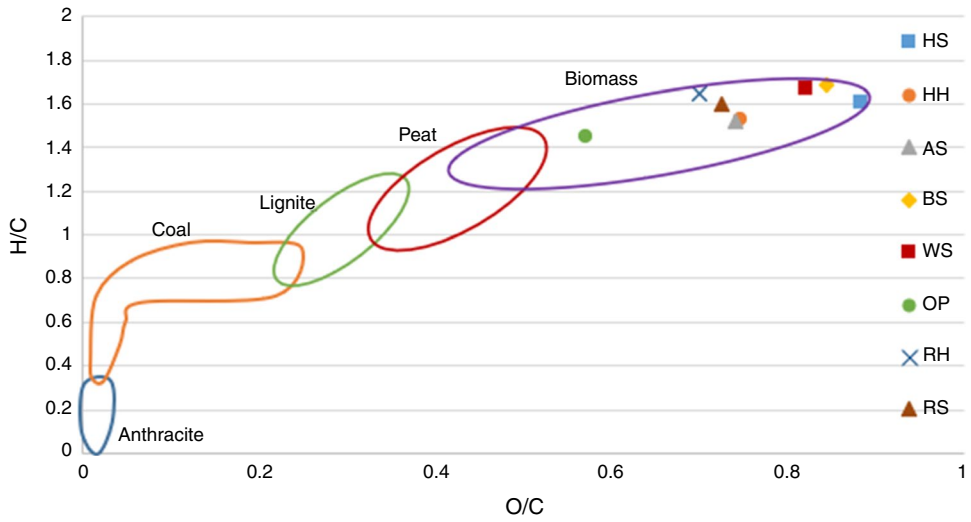

Fig. 1 Characterization of different biomass samples by Van Krevelen diagram

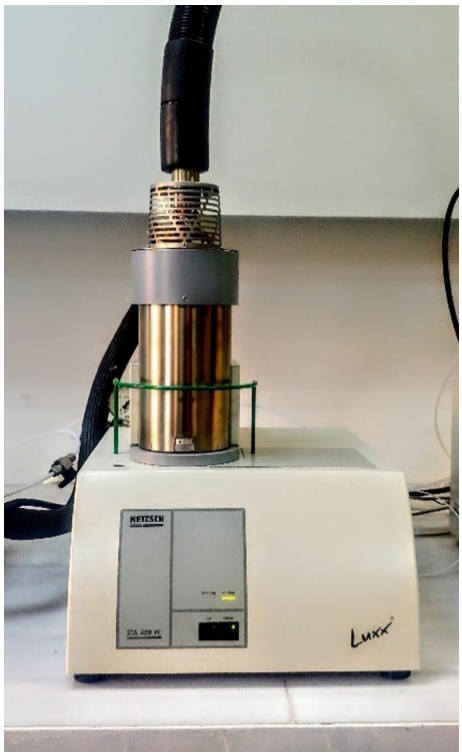

Fig. 2 Netzsch STA 409 PC Luxx

analysis (DTA), TG, derivative thermogravimetric (DTG) curves obtained as a result of the experimental work are shown in Fig. 3.

As shown in Fig. 3, the dashed, dotted dash, and solid lines symbolize the TG, DTG, and DTA curves, respectively. The TG curve represents the mass loss during the combustion process of a sample as a function of temperature and/or time. DTG is a measure of mass change rate (% min^{-1}) that can be used to analyze the TG curves of overlapping reactions and determine zones/steps of the combustion process. On the other hand, DTA is used to classify reactions as exothermic or endothermic based on the temperature difference. As a result of the TG curve analysis, the "ignition temperature" is calculated from the point where mass loss increases, and the "burnout temperature" is determined at the point where mass loss ceases [20]. When the DTG curve was examined, it was found that combustion occurs in two stages, with the first stage burning the volatile matters and the second stage burning the fixed carbon in biomass. The DTA curve shows that both stages of combustion have an exothermic reaction type. In this study, the moisture loss from the sample was neglected and the combustion process was investigated between 200 and 800°C. The "DTG_{max}" point indicates the moment where the highest mass loss occurred during the entire combustion procedure. Biomasses typically lose the majority of their mass in the zone where volatile substances are burned, and "DTG_{max}" is primarily located in this stage.

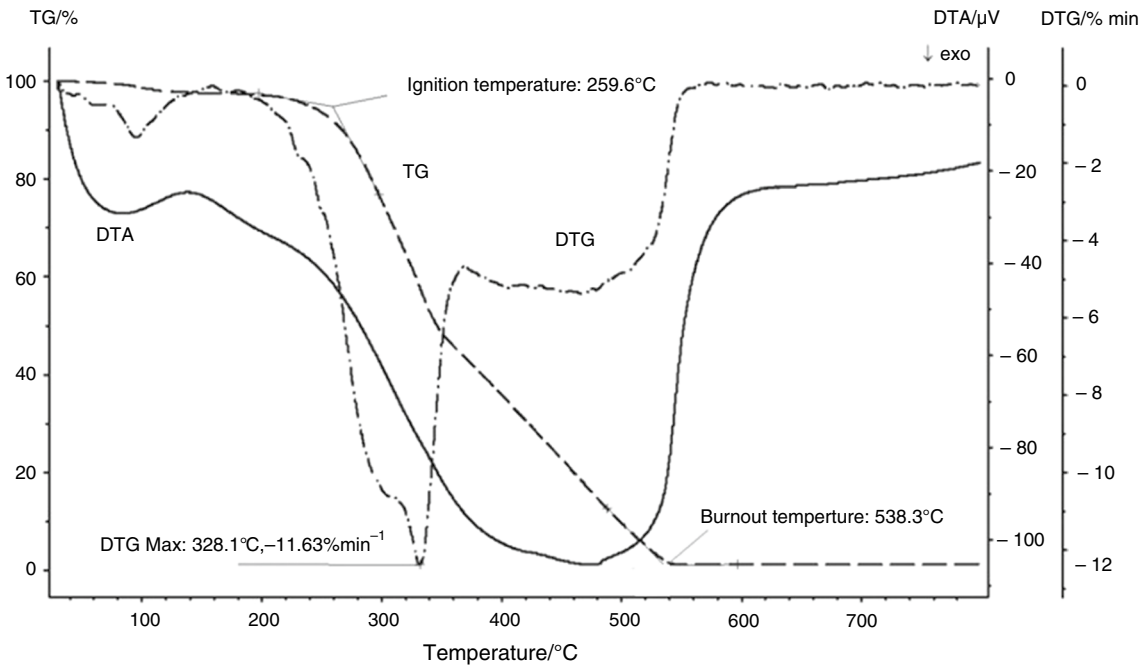

Fig. 3 TG, DTG, and DTA curves for the combustion process of hazelnut shell (20°C min^{-1})

Instantaneous combustion index

Combustion performance of lignocellulosic fuel was determined using parameters from DTG curve and temperature. The instantaneous combustion characteristic index (S_j) can be expressed as follows:

$$S_j = (\mathrm{DTG}_{max} \times (\mathrm{DTG}_j + \mathrm{DTG}_{j-1})/2)/(T_i^2 \times T_b) \quad (2)$$

where "T_i" (°C) is the summation of ignition temperature with 273.15 and "T_b" (°C) is the summation of burnout temperature with 273.15. "DTG_{max}" (% min^{-1}) demonstrates the point where the maximum mass loss takes place, and "DTG_j" (% min^{-1}) is a derivative thermogravimetric value at the temperature of T_j (°C).

Artificial neural networks

ANN represents a distributed and massively parallel information processing system that can handle complicated and nonlinear problems, such as those in engineering. ANN simulates the functions of biological neurons with artificial nodes/neurons that mimic the human brain [21]. ANNs train themselves by using experiences and design a pattern to produce the output. Moreover, ANNs do not produce analytical outputs and only produce numerical results, which make them black-box models [22]. The basic processing element of ANN is an artificial node (neuron) where computations take place and output is determined, and it can be implemented in several ways. The general structure of an artificial neuron is illustrated in Fig. 4.

The results of multiplying the outputs of the neurons of the previous layer (X_i) by their mass value (W_{ji}) are summed with the bias value (B_j). Typically, the initial biases and masses are determined randomly, and the determination of the output of an artificial neuron can be depicted by Eq. 3:

$$\mathrm{out}_j = h\left(\sum_{i=1}^{N} W_{ji}X_i + B_j\right) \quad (3)$$

The activation function (h) comes in numerous forms, such as ReLU, ELU, exponential, logarithmic, and tangent sigmoid. The tangent sigmoid, which is used as the activation function in this study, can be expressed as follows:

$$f(x) = (e^x - e^{-x})/(e^x + e^{-x}) \quad (4)$$

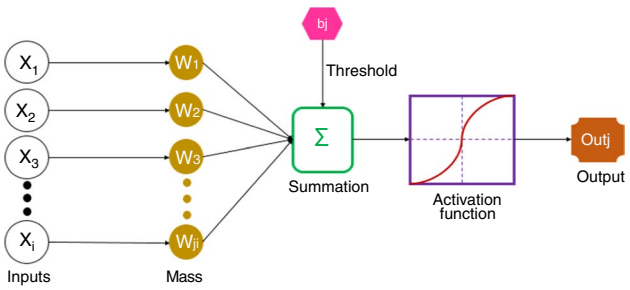

Fig. 4 Structure of an artificial neuron

Bayesian optimization (BO) algorithm was applied to optimize the hyperparameters of the developed ANN model. BO algorithm utilizes the Bayes theorem which is a Gaussian-based optimization procedure calculating the expected probability considering the current observations. BO uses a prior likelihood to converge the posterior probability of the unknown objective function and chooses the next sampled hyperparameter combination according to the distribution. In BO, the masses and biases of the ANN are assigned randomly at the initial, and these parameters are adjusted using a statistical technique which is the mean sum of squared network errors. The BO technique is remarkably superior when the objective function is unknown and the computational complication is high [23].

Performance indicators

The error in ANN is calculated from the difference between the actual values and the predicted values. The loss function, also known as the error measurement for a single training, is critical to the performance of a network because the parameters of a network are ultimately chosen to reduce the loss to the absolute lowest value. The mean squared error (MSE) used as the loss function in this study is given in Eq. 5.

$$\mathrm{MSE} = 1/n \sum_{i=1}^{n} \left(Y_{predicted} - Y_{actual}\right)^2 \quad (5)$$

where "n" is the number of instances, "$Y_{predicted}$" is the estimated value by the ANN model, "Y_{actual}" is the target value, and "Y_{mean}" is the mean value of target outputs. The performance indicators for the combustion index (S) were selected by using the root-mean-square error (RMSE) in Eq. 6, the mean absolute percentage error (MAPE) in Eq. 7, and the coefficient of determination (R^2) in Eq. 8:

$$\mathrm{RMSE} = \sqrt{1/n \sum_{i=1}^{n} \left(Y_{predicted} - Y_{actual}\right)^2} \quad (6)$$

$$\mathrm{MAPE} = 100/n \sum_{i=1}^{n} \left| \frac{Y_{actual} - Y_{predicted}}{Y_{actual}} \right| \quad (7)$$

$$R^2 = 1 - \sum_{i=1}^{n} \left(Y_{predicted} - Y_{actual}\right)^2 / \sum_{i=1}^{n} \left(Y_{predicted} - Y_{mean}\right)^2 \quad (8)$$

Results

TG-DTG analysis

The TGA is often used to understand the combustion mechanism and accordingly characterizes the thermochemical processes [24]. Furthermore, the TGA has the great importance to advance the knowledge about the reactivity for the combustion [25]. Considering the different chemical and physical properties of the biomass samples that can be seen in the proximate and elemental analysis results, thermal decomposition behaviors are expected to be different for each of them. Figure 5 represents the TG, DTG, and DTA curves of biomass samples at heating rate of 40°C min^{-1}.

The thermal decomposition of the biomass sample is observed at the different temperatures using the TG, DTG, and DTA curves. The mass changes take place in two stages that can be named as volatile and fixed carbon combustion zones as shown in the TG, DTG, and DTA curves (Fig. 5 a, b and c). According to the results shown in Fig. 5, first stage of combustion takes place at the temperature between 250 and 380°C and the second stage starts from end of the first stage and continues until the temperature around 750°C. The start and end points, temperature ranges, and mass changes of the volatile and fixed carbon zones have been varied for each samples that can be explained by the ash, volatile matter, and fixed carbon contents of them as seen in the proximate analysis results in Sect. 2.1. The mass losses (%) and residual masses (%) have been derived from TG curves and are listed in Table 2. In the first stage of combustion, the maximum mass change was recorded for the almond shell as 53.77%, whereas the minimum mass change is 38.34% for rice husk because the almond shell has the highest volatile matter content. In the second stage, hazelnut shell has lost 45.10% of its mass. This value is higher than the other biomass samples used in this study, and it can be explained with its highest fixed carbon content. The behavior of decomposition for each sample gave consistent results with literature studies [26].

The biomass samples except olive pomace lost more mass in the volatile combustion zone, and their mass losses per unit time (% min^{-1}) reached the highest value at temperatures 344.7°C (24.45% min^{-1}), 293°C (17.58% min^{-1}), 300.6°C (25.19% min^{-1}), 279.4°C (26.02% min^{-1}), 284.5°C (24.32% min^{-1}), 286.2°C (19.71% min^{-1}), 300.4°C (22.17% min^{-1}), 280.2°C (21.39% min^{-1}) for hazelnut shell, hazelnut husk, almond shell, barley straw, wheat straw, olive pomace, rice husk, and rice straw, respectively. The biomass samples with higher amount of mass changes in the volatile zone have deeper DTG curves that can be seen in Fig. 5b. Mass change of almond shell in the volatile zone is 53.77% which is the highest amount, and it has the deepest DTG curve compared the others accordingly. Moreover, there is no mass change in the biomass samples after about 750°C, which means that the combustion process is finished after this temperature. The residual mass (%) contains mostly ash and less unconverted carbon in the crucible at the end of the combustion. The residual mass for each samples is presented in Table 2. TG curves indicate that amount of residue from the rice husk of 19.76% is the highest amount. Notably, the rice husk sample has the highest ash content and the lowest fixed carbon content compared to the other biomass samples.

The enthalpic events that occur at each step are depicted by DTA curves. Figure 5 c shows a single noticeable curve that corresponds to the exothermic phases of all biomass samples. The exothermic action corresponds to the combustion process, and only one significant curve can be detected in the DTA curve for all biomass samples. The volatile release zone, which corresponds to a temperature range of 200–300°C, demonstrated an endothermic stage with a lower peak than the exothermic stage. From DTA, the curve between 300 and 700°C is related to the reacting of biomass samples with oxygen. Despite the fact that the release of volatiles is an endothermic process, exothermy occurs primarily as a result of the combustion process [27].

ANN model topology

ANN was developed as a beneficial model for learning through artificial intelligence techniques to predict important parameters for specific applications [28, 29]. ANN is a significant approach with its ability to distinguish very complex relationships between the input and output data set according to the performance of the other training methods [30]. As can be seen in Fig. 6, the feedforward backpropagation learning method based on multilayer perceptron (MLP) structure was used in this study, which is very effective in predicting the behavior of nonlinear systems.

The artificial neural network Simulink package in MATLAB (R2020a) was used to build the neural network model and examine the data sets. The total 6721 data sets were divided into 90% for training and 10% for testing to achieve the predictive ability of the ANN model. Input layer consists of 5 neurons which are C, H, and O contents (%) of biomass samples (dry basis), heating rate (°C min^{-1}), and temperature (°C) for combustion process. The number of perceptrons and hidden layers is not determined by any particular approach. These numbers were adjusted to minimize error value by trial and error. The ANN model was optimized when the neuron numbers in the first and second hidden layers are 28 and 4, respectively. The tangent sigmoid

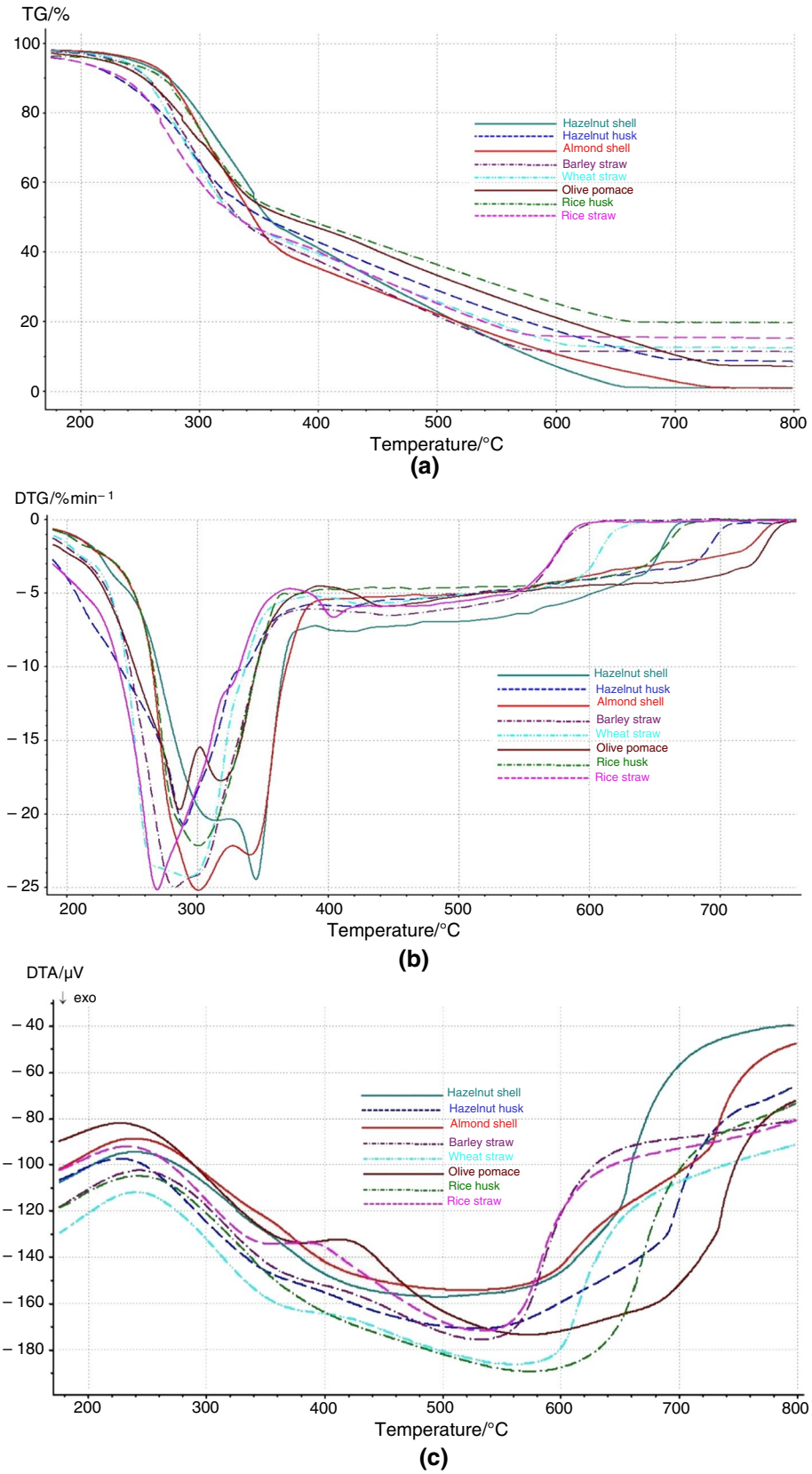

Fig. 5 Curves for the combustion process of the biomass samples at heating rate of 40°C min^{-1}: **a** TG, **b** DTG, and **c** DTA

Table 2 Mass changes and residual mass values for biomass samples

Sample	Volatile zone/%	Fixed carbon zone/%	Residual/%
Hazelnut shell	46.48	45.10	0.91
Hazelnut husk	43.37	40.97	8.50
Almond shell	53.77	37.49	1.01
Barley straw	47.89	33.59	11.40
Wheat straw	46.01	34.72	12.41
Olive pomace	42.58	44.76	7.15
Rice husk	38.34	33.51	19.76
Rice straw	45.66	31.33	15.21

Table 3 The properties of the ANN model

ANN Model	Specification
Learning algorithm	Backpropagation
Optimizer	Bayesian regularization
1. Hidden layer	28 Artificial neurons
2. Hidden layer	4 Artificial neurons
Network	Feed forward
Transfer function	Tangent sigmoid
Data sets number	6721
Training and testing data set split	90%, 10%
Loss function	Mean squared error

was selected as a transfer function in the hidden layers. For each neuron, the masses of the neurons are multiplied by the input signal, and the total value obtained is summed with the bias value and then processed with the tangent sigmoid transfer function. Instantaneous combustion index was predicted using the data transferred from hidden layers to output layer. The BO algorithm was selected as the optimizer due to its ability to work efficiently for the learning of noisy and complicated data sets since minimization of the MSE and avoiding overfitting have been aimed for the well-trained model. Specifications of the ANN model are summarized in Table 3.

Evaluation of ANN model

The training data set was used for the learning process, and the parameters of the ANN model were assigned with iterations. After the training part, the model was tested with the test data set, which did not contain any information about the correlation between the input and output values of the training data set, and the performance of the model was evaluated with the test data. Therefore, the model reached its maximum generalization capacity when the MSE was minimized as a loss function calculated using the estimated

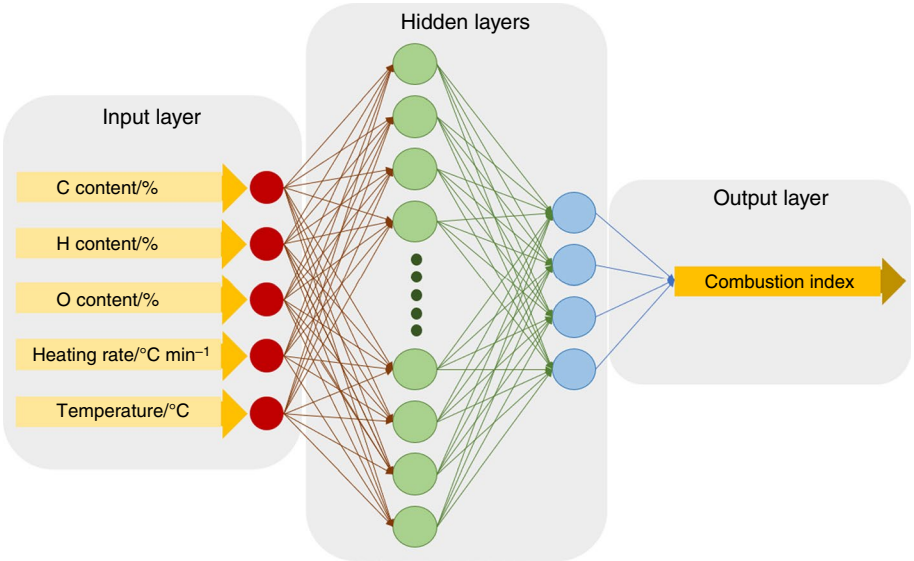

Fig. 6 The structure of the ANN for prediction of combustion index value

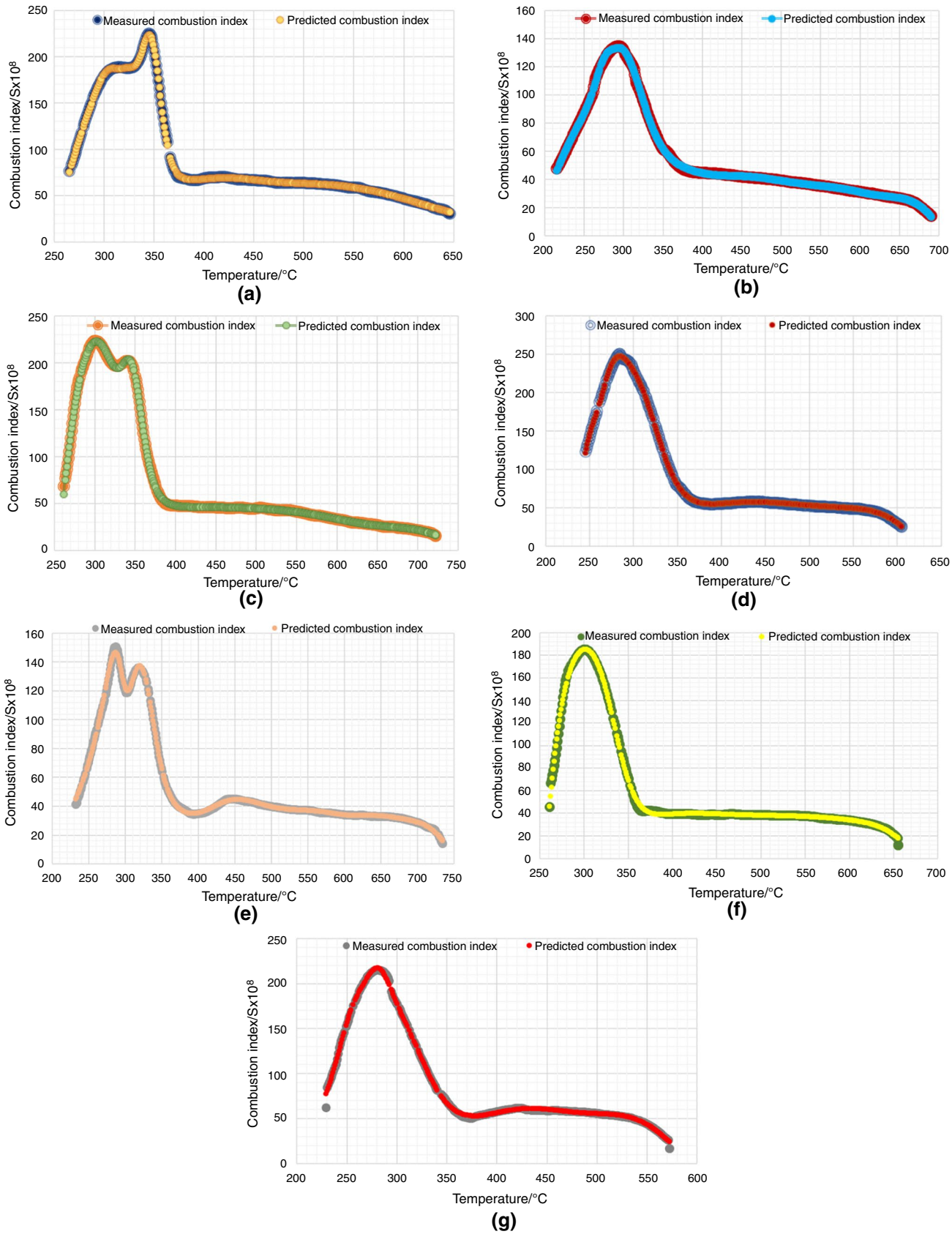

Fig. 7 Change of the combustion index with the temperature at heating rate of 40°C min^{-1} for the training data sets: **a** hazelnut shell, **b** hazelnut husk, **c** almond shell, **d** wheat straw, **e** olive pomace, **f** rice husk, **g** rice straw

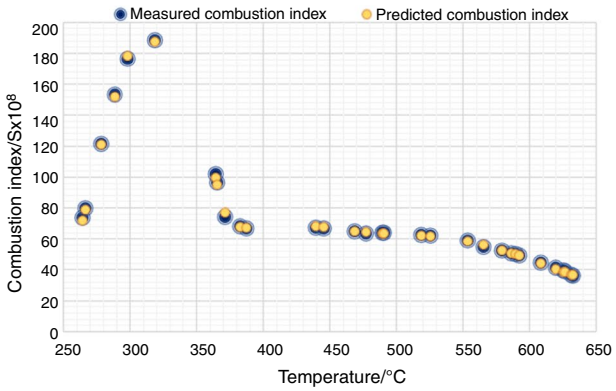
Measured combustion index
Predicted combustion index
Combustion index/Sx10⁸
Temperature/°C

(a)

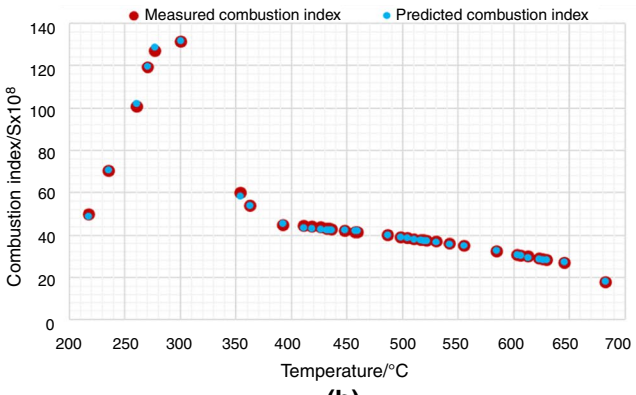
Measured combustion index
Predicted combustion index
Combustion index/Sx10⁸
Temperature/°C

(b)

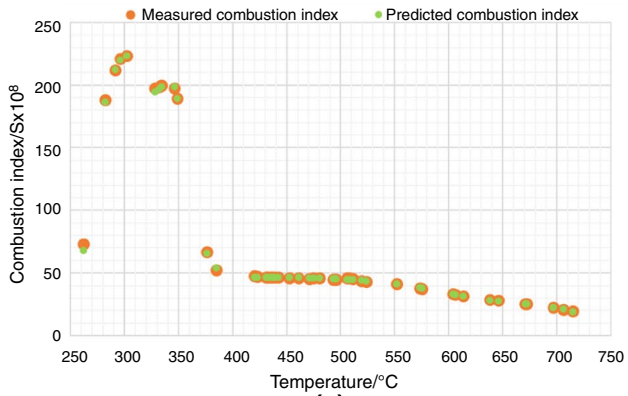
Measured combustion index
Predicted combustion index
Combustion index/Sx10⁸
Temperature/°C

(c)

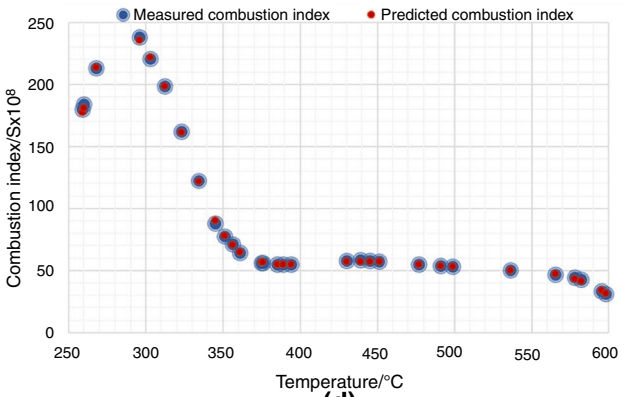
Measured combustion index
Predicted combustion index
Combustion index/Sx10⁸
Temperature/°C

(d)

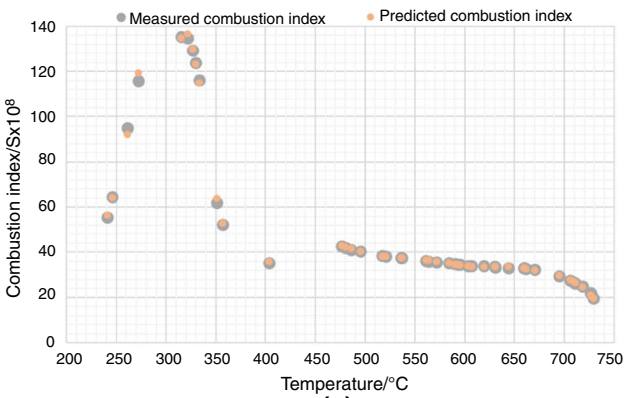
Measured combustion index
Predicted combustion index
Combustion index/Sx10⁸
Temperature/°C

(e)

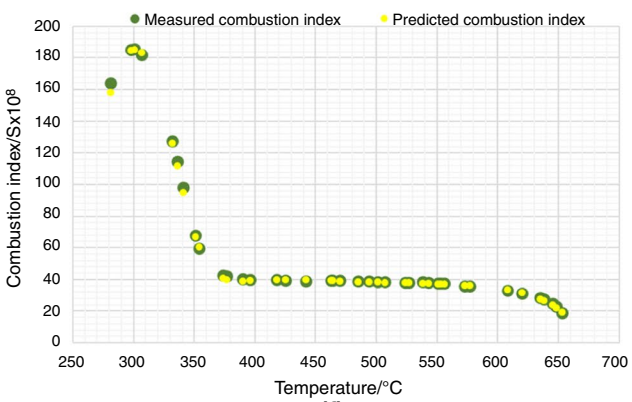
Measured combustion index
Predicted combustion index
Combustion index/Sx10⁸
Temperature/°C

(f)

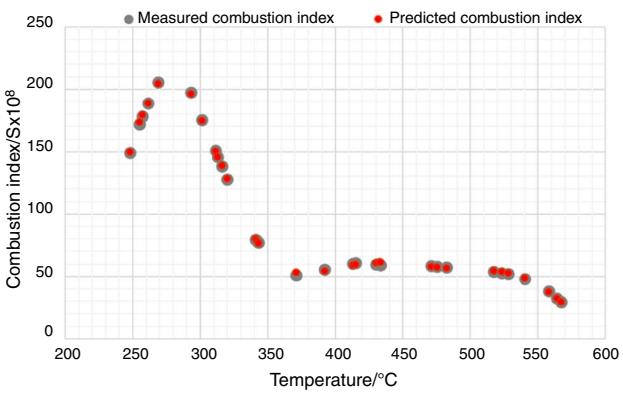
Measured combustion index
Predicted combustion index
Combustion index/Sx10⁸
Temperature/°C

(g)

◂**Fig. 8** Change of the combustion index with the temperature at heating rate of 40°C min^{-1} for the testing data sets: **a** hazelnut shell, **b** hazelnut husk, **c** almond shell, **d** wheat straw, **e** olive pomace, **f** rice husk, **g** rice straw

and measured values of the instantaneous combustion index under the conditions given in Table 3.

RMSE, MAPE, and R^2 were used to assess the predictive capability of the ANN model. The training and testing results were presented for each biomass sample at the heating rate of 40°C min^{-1} in Figs. 7–8. The change in combustion index values as temperature rises was investigated for both measured and predicted data sets.

As a result of Figs. 7–8, measured and predicted instantaneous combustion index values showed similar behavior according to temperature change for training and testing data sets. Their results are quite satisfying because the trend lines of measured and predicted results were the same and overlapped each other. Instantaneous combustion index values for the each biomass sample reached the maximum value when the process temperature increased between 250 and 350°C. This behavior is directly related to the characteristics of the biomass samples that have high volatile matter content [10, 20]. The temperature range corresponds to volatile combustion zone, which is mentioned in Sect. 3.1.

The calculation of the combustion index was started from the ignition temperature and continued until the burnout temperature, and hence, the temperature ranges varied depending on each process. In Fig. 5, instantaneous combustion index values increased as the temperature enhanced between 250 and 350°C. After reaching their maximum value, they sharply decreased from 230×10^8 to 70×10^8, 140×10^8 to 40×10^8, 240×10^8 to 40×10^8, 260×10^8 to 50×10^8, 155×10^8 to 35×10^8, 190×10^8 to 40×10^8, 220×10^8 to 50×10^8 for hazelnut shell, hazelnut husk, almond shell, olive pomace, rice husk, and rice straw, respectively. Fixed carbon combustion started when the temperature value exceeded 350°C. The calculated and predicted combustion index value in the fixed carbon zone is lower than the value in the volatile zone because the volatile components give high energy compared with the other components released in the fixed carbon combustion zone [31]. The instantaneous combustion index almost stabilized for wheat straw, olive pomace, and rice straw; however, it showed slight increased and decreased for hazelnut shell, hazelnut husk, almond shell, rice husk in the temperature between 350°C and 700°C. The prediction capability of ANN model at the heating rate 40°C min^{-1} was examined by using regression coefficient (R^2) which is the important parameter to examine the ANN generalization capability. Results are depicted in Figs. 9–10 for training and testing data sets, respectively.

The results of R^2 plot proved the ANN model successfully estimated the combustion index for training and testing data sets at heating rate of 40°C min^{-1}. R^2 values have been found to be greater than 0.99, which are within satisfactory limits for testing and training data sets. The developed ANN model performance has been examined at different heating rates using R^2, RMSE, and MAPE in Table 4.

Although R^2 values at the heating rate of 10°C min^{-1} were found to be lower than others because of more detailed DTG results, they were still within satisfactory limits. Besides, MAPE and RMSE values were obtained quitely low and acceptable. The RMSE values were calculated less

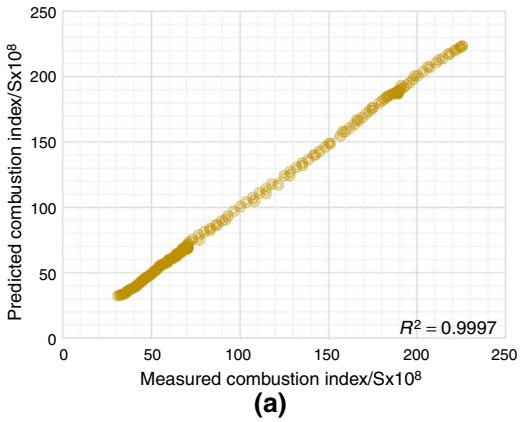
Predicted combustion index/Sx10⁸
Measured combustion index/Sx10⁸
R² = 0.9997
(a)

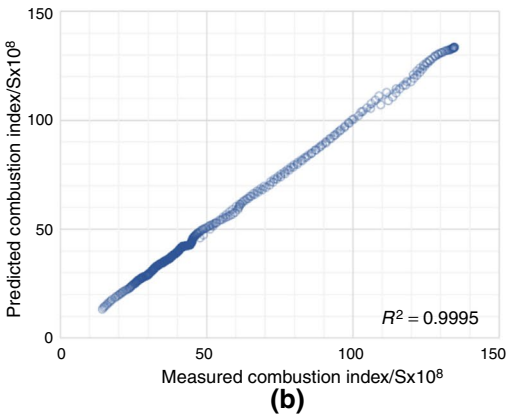
Predicted combustion index/Sx10⁸
Measured combustion index/Sx10⁸
R² = 0.9995
(b)

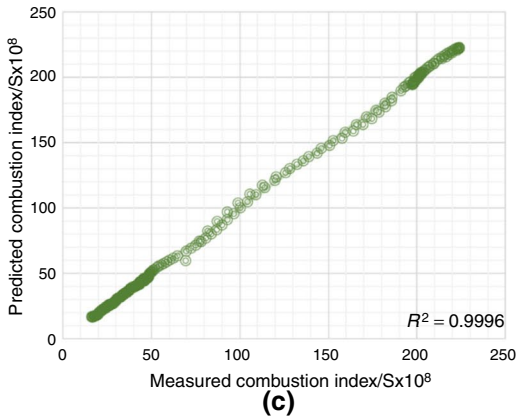
Predicted combustion index/Sx10⁸
Measured combustion index/Sx10⁸
R² = 0.9996
(c)

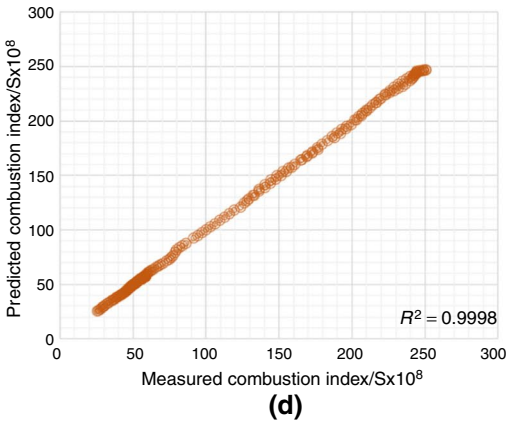
Predicted combustion index/Sx10⁸
Measured combustion index/Sx10⁸
R² = 0.9998
(d)

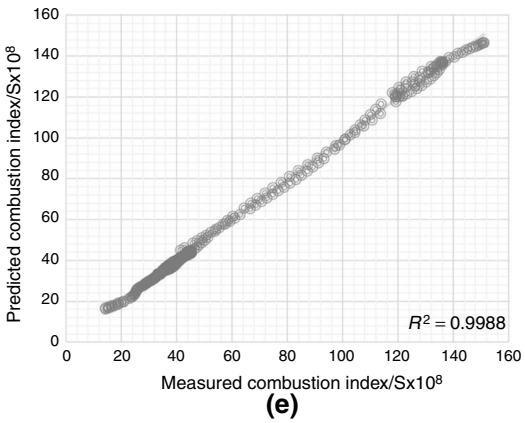
Predicted combustion index/Sx10⁸
Measured combustion index/Sx10⁸
R² = 0.9988
(e)

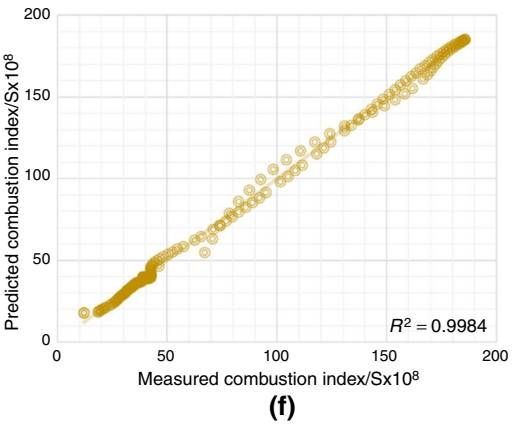
Predicted combustion index/Sx10⁸
Measured combustion index/Sx10⁸
R² = 0.9984
(f)

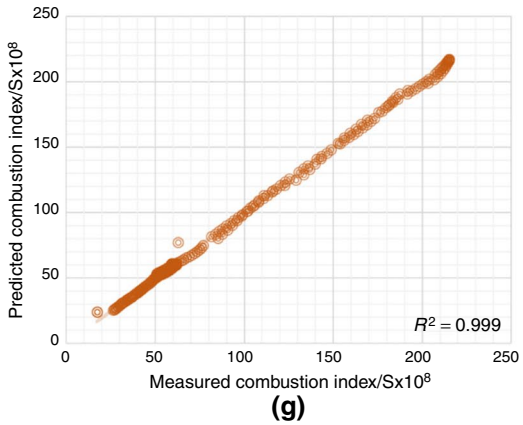
Predicted combustion index/Sx10⁸
Measured combustion index/Sx10⁸
R² = 0.999
(g)

◂**Fig. 9** R^2 values at heating rate of 40°C min^{-1} for the training data sets: **a** hazelnut shell, **b** hazelnut husk, **c** almond shell, **d** wheat straw, **e** olive pomace, **f** rice husk, **g** rice straw

than 5.7278, and the MAPE values changed between 0.6729 and 6.8504 except the experiment of almond shell at heating rate of 10°C min^{-1}.

Results showed that the model had been created with high prediction capability without overfitting. Hereby, the combustion index values for each biomass sample at heating rates of 10, 20, and 40°C min^{-1} were well estimated.

External validation of the ANN model

Model evaluation results according to the R^2, MAPE, and RMSE have been shown reliable performance to predict the combustion index value of each heating rate for selected biomass samples. In this section, the ANN model was tested with barley straw as an external validator, which has a completely different content of C, H, and O. In addition to the results of the elemental analysis, barley straw also has different contents of ash, fixed carbon, and volatile matter, as mentioned in Sect. 2.1. The results estimated from the ANN model for the combustion index values of barley straw combustion are presented in Fig. 11 in comparison with the measured combustion index values.

The change in the combustion index with the temperature showed similar behavior for the predicted and measured data sets with slight deviations. Results indicated that the combustion index exceeded 300×10^8 for the first time compared with the training and test results of each biomass sample with a heating rate of 40°C min^{-1}. This proves that the ANN model is able to predict the value not yet seen in the training part. Prediction results for the barley straw sample were also evaluated with R^2, MAPE, and RMSE in Table 5.

R^2 value for the performance validation sample was found to be greater than 0.9843 as shown in Table 5. Additionally, the RMSE and MAPE values for the combustion index prediction were calculated 10.9956 and 9.5996, respectively.

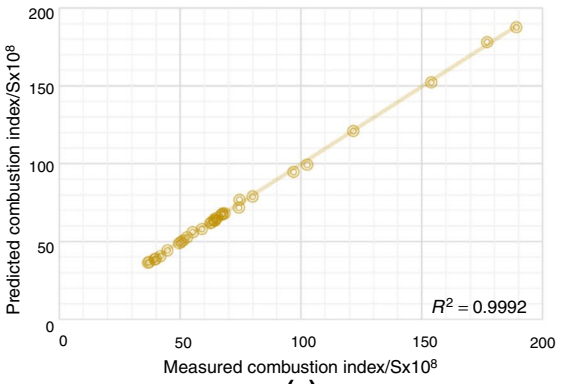
Predicted combustion index/Sx10⁸
Measured combustion index/Sx10⁸
R² = 0.9992
0
50
100
150
200

(a)

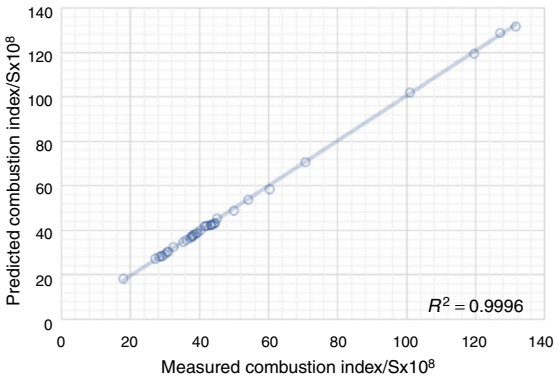
Predicted combustion index/Sx10⁸
Measured combustion index/Sx10⁸
R² = 0.9996
0
20
40
60
80
100
120
140

(b)

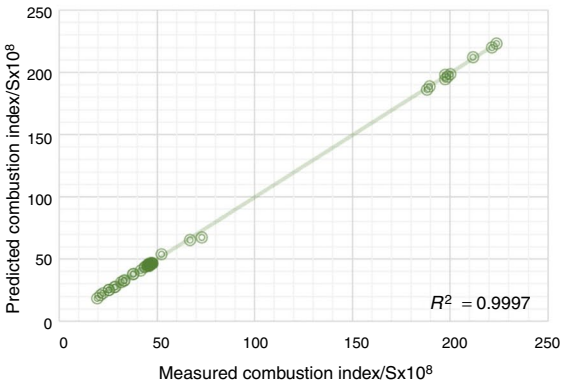
Predicted combustion index/Sx10⁸
Measured combustion index/Sx10⁸
R² = 0.9997
0
50
100
150
200
250

(c)

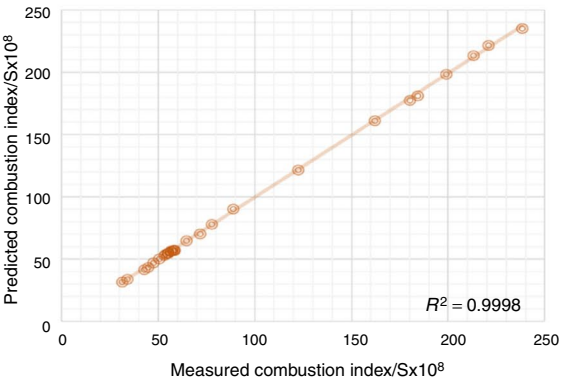
Predicted combustion index/Sx10⁸
Measured combustion index/Sx10⁸
R² = 0.9998
0
50
100
150
200
250

(d)

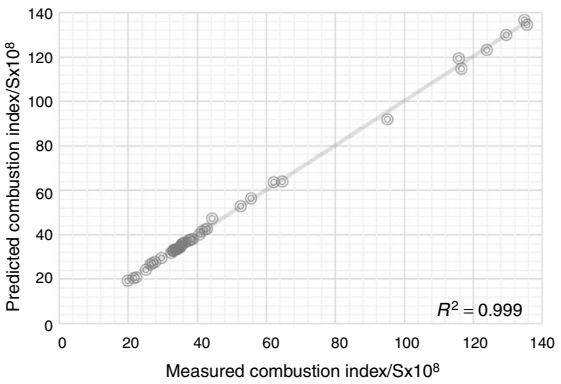
Predicted combustion index/Sx10⁸
Measured combustion index/Sx10⁸
R² = 0.999
0
20
40
60
80
100
120
140

(e)

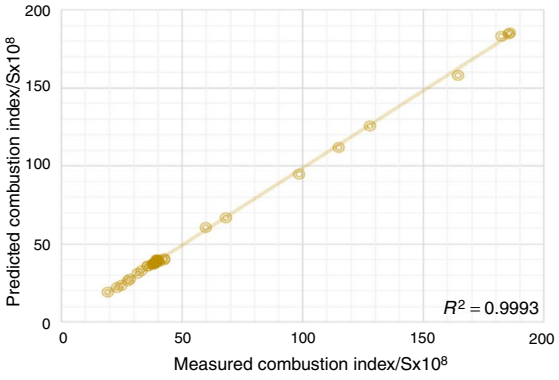
Predicted combustion index/Sx10⁸
Measured combustion index/Sx10⁸
R² = 0.9993
0
50
100
150
200

(f)

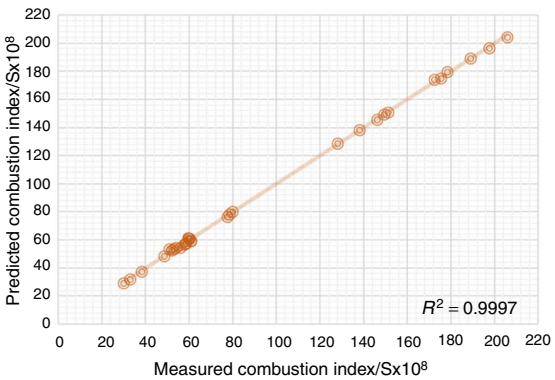
Predicted combustion index/Sx10⁸
Measured combustion index/Sx10⁸
R² = 0.9997
0
20
40
60
80
100
120
140
160
180
200
220

(g)

◂**Fig. 10** R^2 values at heating rate of 40°C min^{-1} for the testing data sets: **a** hazelnut shell, **b** hazelnut husk, **c** almond shell, **d** wheat straw, **e** olive pomace, **f** rice husk, **g** rice straw

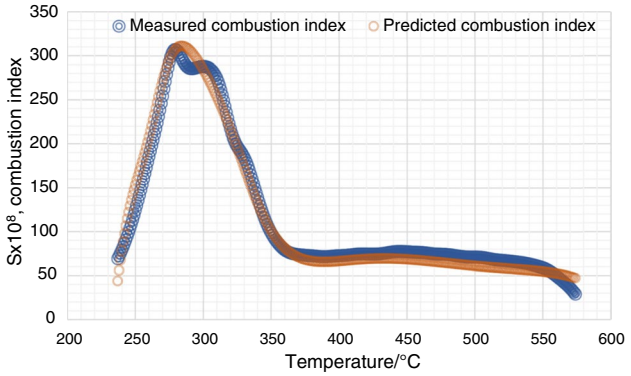

Fig. 11 Variation of combustion index with a heating rate of 40°C min^{-1} for the measured and predicted data sets of the external validator (barley straw)

Table 5 R^2, MAPE, and RMSE results of barley straw

Sample	Heating Rate/°C min^{-1}	R^2	RMSE	MAPE
Barley straw	40	0.9843	10.9956	9.5996

These results are sufficient to demonstrate the reliability of the proposed model. This means that the developed ANN model works efficiently to predict the combustion index for biomass combustion processes.

Table 4 Performance results for the combustion index prediction of training and testing data sets at different heating rates using R^2, RMSE, and MAPE

Sample	Heating rate/°C min^{-1}	Training data set			Testing data set		
		R^2	RMSE	MAPE	R^2	RMSE	MAPE
Hazelnut shell	10	0.9246	1.3839	6.3198	0.9498	0.9285	6.8504
	20	0.9966	0.7706	1.6692	0.9959	0.9234	2.2148
	40	0.9997	0.9221	0.8462	0.9992	1.0490	1.0177
Hazelnut husk	10	0.9708	0.6085	5.8052	0.9630	0.5752	6.1948
	20	0.9940	0.7429	2.6879	0.9905	0.9428	3.3146
	40	0.9995	0.6922	0.9474	0.9996	0.6303	0.9751
Almond shell	10	0.8438	2.8178	9.6228	0.8572	4.0902	13.4262
	20	0.9624	5.1833	5.1470	0.9859	5.7278	5.0017
	40	0.9996	1.2546	1.1762	0.9997	1.0958	1.0706
Wheat straw	10	0.9958	0.4520	4.2094	0.9871	0.4937	5.4972
	20	0.9983	0.9369	2.7433	0.9982	0.9894	2.9778
	40	0.9998	0.8742	0.6729	0.9998	1.0292	0.8955
Olive pomace	10	0.9767	0.4317	5.8769	0.9662	0.4452	5.6386
	20	0.9957	0.6196	3.1197	0.9983	0.4432	1.9739
	40	0.9988	1.1762	1.4299	0.9990	1.0239	1.2165
Rice husk	10	0.9924	0.4293	4.8195	0.9940	0.4134	4.4772
	20	0.9964	0.9755	3.7403	0.9969	0.8238	3.2206
	40	0.9984	1.8852	2.1469	0.9993	1.3764	1.6245
Rice straw	10	0.9933	0.4174	3.6033	0.9920	0.4399	3.6414
	20	0.9966	0.9087	2.3042	0.9975	0.5670	2.2255
	40	0.9990	1.6827	1.8269	0.9997	1.0476	1.2762

Conclusions

This study emphasizes the implementation of a machine learning approach using ANN to characterize combustion, which provides direction for selecting the correct path for systematic design of each thermal plant to reduce the experimental time. Thus, the prediction of the instantaneous combustion index provides an alternative approach. In this study, the predicted and measured combustion index values corresponding to temperature were compared and a similar trend was found. Correlation coefficients were obtained greater than 0.99 for testing and training data sets and 0.98 for the external validation sample at heating rate of 40°C min^{-1}.

Supplementary Information The online version contains supplementary material available at https://doi.org/10.1007/s10973-022-11208-8.

Author contributions UO contributed to conceptualization, formal analysis, methodology, project administration, resources, and supervision. SS, FK, and UO were equally involved in data curation, investigation, and writing—review and editing. SS and UO provided software equally and contributed equally to validation, visualization, and writing—original draft preparation,

References

1. Abokyi E, Appiah-Konadu P, Abokyi F, Oteng-Abayie EF. Industrial growth and emissions of CO2 in Ghana: the role of financial development and fossil fuel consumption. Energy Rep. 2019;5:1339–53.
2. Okolie JA, Nanda S, Dalai AK, Berruti F, Kozinski JA. A review on subcritical and supercritical water gasification of biogenic, polymeric and petroleum wastes to hydrogen-rich synthesis gas. Renew Sustain Energy Rev. 2020;119:109546.
3. Ravanchi MT, Sahebdelfar S. Catalytic conversions of CO2 to help mitigate climate change: recent process developments. Process Saf Environ Prot. 2021;145:172–94.
4. Phanphanich M, Mani S. Impact of torrefaction on the grindability and fuel characteristics of forest biomass. Biores Technol. 2011;102(2):1246–53.
5. Kanca A. Investigation on pyrolysis and combustion characteristics of low quality lignite, cotton waste, and their blends by TGA-FTIR. Fuel. 2020;263:116517.
6. Mureddu M, Dessì F, Orsini A, Ferrara F, Pettinau A. Air-and oxygen-blown characterization of coal and biomass by thermogravimetric analysis. Fuel. 2018;212:626–37.
7. Haykiri-Acma H, Yaman S. Interaction between biomass and different rank coals during co-pyrolysis. Renew Energy. 2010;35(1):288–92.
8. Li X, Miao W, Lv Y, Wang Y, Gao C, Jiang D. TGA-FTIR investigation on the co-combustion characteristics of heavy oil fly ash and municipal sewage sludge. Thermochim Acta. 2018;666:1–9.
9. Shan F, Lin Q, Zhou K, Wu Y, Fu W, Zhang P, et al. An experimental study of ignition and combustion of single biomass pellets in air and oxy-fuel. Fuel. 2017;188:277–84.
10. Wang G, Zhang J, Shao J, Liu Z, Zhang G, Xu T, et al. Thermal behavior and kinetic analysis of co-combustion of waste biomass/low rank coal blends. Energy Convers Manage. 2016;124:414–26.
11. Fernandez-Lopez M, Puig-Gamero M, Lopez-Gonzalez D, Avalos-Ramirez A, Valverde J, Sanchez-Silva L. Life cycle assessment of swine and dairy manure: pyrolysis and combustion processes. Biores Technol. 2015;182:184–92.
12. Farrow ST, Sun C, Liu H, Le Manquais K, Snape CE. Comparative study of the inherent combustion reactivity of sawdust chars produced by TGA and in the drop tube furnace. Fuel Process Technol. 2020;201:106361.
13. Poomsawat S, Poomsawat W. Analysis of hydrochar fuel characterization and combustion behavior derived from aquatic biomass via hydrothermal carbonization process. Case Stud Therm Eng. 2021;27:101255.
14. Ma B-G, Li X-G, Xu L, Wang K, Wang X-G. Investigation on catalyzed combustion of high ash coal by thermogravimetric analysis. Thermochim Acta. 2006;445(1):19–22.
15. Opfermann J, Kaisersberger E, Flammersheim H. Model-free analysis of thermoanalytical data-advantages and limitations. Thermochim Acta. 2002;391(1–2):119–27.
16. Xie C, Liu J, Zhang X, Xie W, Sun J, Chang K, et al. Co-combustion thermal conversion characteristics of textile dyeing sludge and pomelo peel using TGA and artificial neural networks. Appl Energ. 2018;212:786–95.
17. Chen J, Liu J, He Y, Huang L, Sun S, Sun J, et al. Investigation of co-combustion characteristics of sewage sludge and coffee grounds mixtures using thermogravimetric analysis coupled to artificial neural networks modeling. Biores Technol. 2017;225:234–45.
18. Díaz-Faes E, Barriocanal C, Diez M, Alvarez R. Applying TGA parameters in coke quality prediction models. J Anal Appl Pyrol. 2007;79(1–2):154–60.
19. Çepelioğullar Ö, Mutlu İ, Yaman S, Haykiri-Acma H. Activation energy prediction of biomass wastes based on different neural network topologies. Fuel. 2018;220:535–45.
20. Lu J-J, Chen W-H. Investigation on the ignition and burnout temperatures of bamboo and sugarcane bagasse by thermogravimetric analysis. Appl Energy. 2015;160:49–57.
21. Diamantopoulou MJ, Milios E, Doganos D, Bistinas I. Artificial neural network modeling for reforestation design through the dominant trees bole-volume estimation. Nat Resour Model. 2009;22(4):511–43.
22. Zaidan MA, Wraith D, Boor BE, Hussein T. Bayesian proxy modelling for estimating black carbon concentrations using white-box and black-box models. Appl Sci. 2019;9(22):4976.
23. Zhou J, Qiu Y, Zhu S, Armaghani DJ, Khandelwal M, Mohamad ET. Estimation of the TBM advance rate under hard rock conditions using XGBoost and Bayesian optimization. Undergr Space. 2020. https://doi.org/10.1016/j.undsp.2020.05.008.
24. Morin M, Pécate S, Masi E, Hémati M. Kinetic study and modelling of char combustion in TGA in isothermal conditions. Fuel. 2017;203:522–36.
25. Yanfen L, Xiaoqian M. Thermogravimetric analysis of the co-combustion of coal and paper mill sludge. Appl Energy. 2010;87(11):3526–32.
26. Wang Q, Wang G, Zhang J, Lee J-Y, Wang H, Wang C. Combustion behaviors and kinetics analysis of coal, biomass and plastic. Thermochim Acta. 2018;669:140–8.
27. Pécora AA, Ávila I, Lira CS, Cruz G, Crnkovic PM. Prediction of the combustion process in fluidized bed based on physical–chemical properties of biomass particles and their hydrodynamic behaviors. Fuel Process Technol. 2014;124:188–97.
28. Yahya HSM, Abbas T, Amin NAS. Optimization of hydrogen production via toluene steam reforming over Ni–Co supported modified-activated carbon using ANN coupled GA and RSM. Int J Hydrog Energy. 2020. https://doi.org/10.1016/j.ijhydene.2020.05.033.
29. Esonye C, Onukwuli OD, Ofoefule AU. Optimization of methyl ester production from Prunus Amygdalus seed oil using response

surface methodology and artificial neural networks. Renew Energy. 2019;130:61–72.
30. Ghasemzadeh K, Ahmadnejad F, Aghaeinejad-Meybodi A, Basile A. Hydrogen production by a PdAg membrane reactor during glycerol steam reforming: ANN modeling study. Int J Hydrogen Energy. 2018;43(15):7722–30.
31. Xinjie L, Singh S, Yang H, Wu C, Zhang S. A thermogravimetric assessment of the tri-combustion process for coal, biomass and polyethylene. Fuel. 2020;287:119355.